Optimization of abdominal CT based on a model of total risk minimization by putting radiation risk in perspective with imaging benefit

Check for updates

Francesco Ria [1] ✉, Anru R. Zhang[2], Reginald Lerebours[2], Alaattin Erkanli[2], Ehsan Abadi[1], Daniele Marin[3] & Ehsan Samei[1]

Abstract

Background Risk-versus-benefit optimization required a quantitative comparison of the two. The latter, directly related to effective diagnosis, can be associated to clinical risk. While many strategies have been developed to ascertain radiation risk, there has been a paucity of studies assessing clinical risk, thus limiting the optimization reach to achieve a minimum total risk to patients undergoing imaging examinations. In this study, we developed a mathematical framework for an imaging procedure total risk index considering both radiation and clinical risks based on specific tasks and investigated diseases.

Methods The proposed model characterized total risk as the sum of radiation and clinical risks defined as functions of radiation burden, disease prevalence, false-positive rate, expected life-expectancy loss for misdiagnosis, and radiologist interpretative performance (i.e., AUC). The proposed total risk model was applied to a population of one million cases simulating a liver cancer scenario.

Results For all demographics, the clinical risk outweighs radiation risk by at least 400%. The optimization application indicates that optimizing typical abdominal CT exams should involve a radiation dose increase in over 90% of the cases, with the highest risk optimization potential in Asian population (24% total risk reduction; 306% $CTDI_{vol}$ increase) and lowest in Hispanic population (5% total risk reduction; 89% $CTDI_{vol}$ increase).

Conclusions Framing risk-to-benefit assessment as a risk-versus-risk question, calculating both clinical and radiation risk using comparable units, allows a quantitative optimization of total risks in CT. The results highlight the dominance of clinical risk at typical CT examination dose levels, and that exaggerated dose reductions can even harm patients.

Plain language summary

The proper practice of radiology (using imaging technology to diagnose and treat diseases) should take into consideration both the risk and benefit to a patient. Such a comparison can be hard because risk and benefit are measured in different ways. The risk includes some amount of radiation exposure to patients which can cause harm, but the benefit could be identifying a medical problem that needs attention. To overcome this obstacle, we developed a mathematical model describing the risk-to-benefit of a medical imaging study. Our modeling exercise found that the clinical benefit outweighs the radiation risk. The finding that benefit of detecting a problem is worth the risk of imaging is contrary to common belief. This study shows that so much emphasis could be put on radiation safety in imaging that avoiding imaging could negatively impact patients' path of care.

Decision making in medicine is based on the benefit-to-risk ratio of a planned procedure. In radiology, this is reflected in the application of justification and optimization principles[1,2]. In particular, justification implies the characterization that the benefit of a radiological procedure outweighs any potential risk, while optimization aims to maximize the benefit over risk, particularly the radiation risk associated with the procedure[2]. Therefore, the proper practice of radiology should take into consideration the simultaneous and quantitative assessment of both radiation risk and benefit of a procedure. However, this has been a major challenge as the risk and benefit rarely use comparable units[3]. The need for optimization is particularly relevant in Computed Tomography (CT) as the leading source of radiation exposure per capita in the US[4].

To characterize radiation risk, many metrics and surrogates have been developed with different degrees of appropriateness[5–7]. These include

[1]Carl E. Ravin Advanced Imaging Labs, Center for Virtual Imaging Trials, Department of Radiology, Duke University Health System, Durham, NC, USA. [2]Department of Biostatistics & Bioinformatics and Department of Computer Science, Duke University, Durham, NC, USA. [3]Department of Radiology, Duke University Health System, Durham, NC, USA. ✉e-mail: francesco.ria@duke.edu

Computed Tomography Dose Index ($CTDI_{vol}$), Effective dose, and Risk Index (RI). $CTDI_{vol}$ and its derivatives (e.g., Size-Specific Dose Estimate and Dose length Product) reflect radiation output in standardized phantoms, and have been used as surrogate metrics of risk in the absence of more representative alternatives. Effective dose offers a more risk-representative, but does not account for patient age and sex. Risk Index (RI), which includes age-, sex-, and tissue-specific risk coefficients, is currently the closest metric to represent the patient radiation burden in CT.

To characterize imaging benefit, one may quantify the benefit of a radiological procedure in term of the anticipated theoretical image quality (e.g., detectability index[8–10]) as a proxy of the potential for a more precise characterization of disease or the lack thereof. Better, imaging benefit can be quantified in terms of the clinical outcome associated with an effective diagnosis[11]. However, these benefit metrics have different units than those associated with radiation risk and thus cannot be put in perspective with radiation risk and thus used for justification or optimization in purposes. This lack is perhaps the primary reason why optimization of radiological procedures tends to be one-sided and strongly biased towards radiation risk only. One may, however, estimate the likelihood of a misdiagnosis, the reciprocal of the benefit conceptualizing a so-called clinical risk. This enables the comparison of radiation and clinical risk with comparable units, thus allowing optimization of an imaging procedure. This idea was postulated in 2018[3], but has not yet been demonstrated for a clinical scenario.

The purpose of this study was to develop a mathematical model to estimate a total risk index considering the radiation risk and clinical benefit of a CT imaging procedure undergoing abdominal exam. The model was tested on a population of one million digital twins simulating the clinical cancer scenario of detecting liver cancer. The study assessed a total risk as functions of the radiation burden, the prevalence of the disease, the false positive rate, the expected life-expectancy loss for an incorrect diagnosis, and the radiologist interpretative performance. The results highlight that, for all demographics, the clinical risk outweighs radiation risk by at least 400%, and that optimizing typical abdominal CT exams should involve a radiation dose increase in over 90% of the cases. At typical CT examination dose levels, clinical risk is highly dominant, and exaggerated dose reductions can even harm patients.

Methods
Total risk formalism
In this study, the total risk (R_t) associated with a CT procedure is characterized as the additive risk of radiation risk (R_r) and clinical risk (R_c):

$$R_t = R_r + R_c. \tag{1}$$

The radiation risk is defined as

$$R_r = p \times s \times RI \times (1 + \beta), \tag{2}$$

where p is the prevalence of the considered disease in a CT population calculated as the ratio of patients diagnosed with the considered disease and patients undergoing a CT exam after referral for symptoms that might be associated with the same pathology; RI is the risk index as described by Li et al. calculated by applying to each organ the age-, sex-, and tissue-specific lifetime attributable risk of cancer incidence coefficients reported in BEIR VII publication[12,13]; s is the 5-year survival rate for a new cancer as reported by the National Cancer Institute Surveillance, Epidemiology, and End Results Program (NCI-SEER), recorded as 68.7% at the time of the manuscript preparation[14]; and β is the false positive to true positive ratio for the detection of the investigated pathology. The $(1 + \beta)$ factor implies that, in case of a false positive, the patient will probably undergo a further CT examination during his path or care.

The clinical risk is defined as

$$R_c = p \times \alpha \times (1 - \beta). \tag{3}$$

The $(1 - \beta)$ factor implies the clinical risk is null under a false positive result, whereas the parameter α describes the expected life-expectancy loss for an incorrect diagnosis as the predicted years of survival for a correct diagnosis minus the predicted years of survival for an incorrect diagnosis. The α parameter was calculated per each race, sex, and age group based on the survival rates for different tumor stages reported by the NCI-SEER program[14].

Combining Eqs. (1), (2), and (3), the resulting total risk is estimated as

$$R_t = p \times [s \times RI \times (1 + \beta) + \alpha \times (1 - \beta)]. \tag{4}$$

Equation (4) provides the total risk associated with a radiological procedure including factors for the radiation burden for different age and sex, the prevalence of the disease, the false positive rate, and the expected life-expectancy loss for an incorrect diagnosis including the effects of age, sex, and race.

Extension of total risk concept to cancer cases
In case of an oncological disease, the stage of the cancer is indicated with k, where $k = 0$ indicates no tumor, and $k = 1, 2, 3$ are related to localized, regional, and distant stages, respectively. Therefore, p_k represents the prevalence of each tumor stage in a clinical CT population with p_0 being the prevalence of non-tumor cases, and α_k represents the expected life-expectancy loss for the incorrect diagnosis per each tumor stage with $\alpha_0 = 0$ and α_k is the predicted years of survival for stage k minus the predicted years of survival for stage $k + 1$.

β_k represents the false positive to true positive ratio for the detection of the stage k of the considered tumor. β_k can be inferred from the Receiver Operating Characteristic curve (ROC) via a simply polynomial fit as

$$\beta_k = \beta_0^{\gamma}, \tag{5}$$

where $ROC(\gamma_k) = x^{\gamma_k}$ or $AUC_k = \int_0^1 x^{\gamma_k} dx$, resulting in

$$\gamma_k = \frac{1}{AUC_k} - 1. \tag{6}$$

From Eqs. (5) and (6) it follows that

$$\beta_k = (\beta_0)^{\left(\frac{1}{AUC_k} - 1\right)}. \tag{7}$$

Finally, Eqs. (4) and (7) together yield:

$$R_t = p_0 \times s \times RI \times (1 + \beta_0) + \sum_{(k>1)} p_k \times \alpha_k \times \left(1 - \beta_0^{\left(\frac{1}{AUC_k} - 1\right)}\right). \tag{8}$$

The values of p_k, α_k, β_0, and AUC_k can be retrieved from literature, historical record, and any other validated source.

Demonstration to a digital twin liver cancer population
To demonstrate the feasibility of the described model in clinical practice, Eq. (8) was applied to a population of one million cases simulating a liver cancer scenario. The demographic information was taken from the publicly available 2019 Census Population Estimates by Age, Sex, Race, and Hispanic Origin[15]. In particular, The United States Census Bureau presents race and ethnic categories as separate questions, and data are collected based on self-identification. The patient population was simulated in eight different cohorts with genders of male and female, and races/ethnicities of white, Black, Hispanic, and Asian. The total population sample size allowed the inclusion of a considerable number of cases in each group. For each simulated patient, the age was randomly sampled from a uniform distribution, which spanned the age range of the individual demographic groups. Because the study involved only simulated digital twins, IRB approval was not required.

Concerning patient body habitus, for each of the eight separate demographic cohorts, the waist diameter in centimeters was randomly sampled per

patient from a truncated normal distribution with mean and standard deviation based on their demographic information (age, sex, and race). The waist circumferences means and their standard errors were obtained from the publicly available Center for Disease Control and Prevention Anthropometric Reference Data for Children and Adults: United States 2015–2018[16]. The standard errors of the means were converted to standard deviations that, together with the means, were multiplied by $1/\pi$ to obtain the sampling distribution of diameter. The normal distributions were truncated to 0 for the lower bound, and the 95th percentile value plus 15 cm for the upper bound.

The CT scanner radiation output was obtained per each simulated case in terms of volume CTDI ($CTDI_{vol}$). The administered $CTDI_{vol,0}$ was calculated using the well-established exponential relationship between patient diameter and $CTDI_{vol}$, and applying the fitting coefficients extracted from a clinical population of 735 patients undergoing abdominopelvic CT with a maximum upper bound $CTDI_{vol}$ of 50 mGy[7]. Table 1 reports the number of cases, age, waist diameter, and utilized $CTDI_{vol}$ for the simulated population per sex and race/ethnicity group.

The cancer incidence and expected life expectancy in terms of 5-year survival rate for each case per different sex, race/ethnicity, age, and stage of diagnosis was extracted from the NCI-SEER. The total risk ($R_{t,0}$) was calculated for a typical false positive to true positive ratio of $\beta_0 = 5\%$ and it was assumed that each case received an average radiologist interpretative performance of $AUC_0 = 0.75$ for a hypothetical lesion without any changes in radiation dose beyond routine practice[17].

To explore the potential use of the framework for imaging optimization (radiation dose minimization), 2000 imaging conditions were simulated for each patient while varying $CTDI_{vol}$ from 0.1 and 200 mGy with 0.1 mGy increments. Per each $CTDI_{vol}$ value, the anticipated area under the receiver operating characteristic curve (AUC) was calculated by applying an expected asymptotic relationship between $CTDI_{vol}$ and image quality[18] as:

$$AUC \propto \frac{1}{2} + \frac{1}{2} erf\left(\frac{q}{2}\right), \tag{9}$$

where q represents an image quality surrogate of diagnostic quality (e.g., detectability index, or signal to noise ratio)[18,19], and erf is the error function. Expecting $q^2 \propto CTDI_{vol}$, Eq. (9) was re-written as

$$AUC = \frac{1}{2} + \frac{1}{2} erf\left(\frac{1}{2}\sqrt{t\frac{CTDI_{vol}}{CTDI_{vol,0}}}\right), \tag{10}$$

where t represents a parameter returning the arbitrary AUC_0 when $CTDI_{vol} = CTDI_{vol,0}$

$$t = 4\left(inverf\left(2AUC_0 - 1\right)\right)^2, \tag{11}$$

where $inverf$ is the inverse function of erf. For this study, $t\left(AUC_0 = 0.75\right) = 0.90987$.

The AUC values distribution generated after applying Eq. (10) to the 2000 imaging conditions per each patient was inputted in Eq. (8) to calculate the total risk distribution. The analytical minimum of such distribution represented the theoretical minimum total risk $R_{t,min}$ for the patient with the related $CTDI_{vol,min}$ representing the theoretical radiation dose that should be administered to minimize the overall total risk. Percentage differences between $R_{t,min}$ and $R_{t,0}$, and between $CTDI_{vol,min}$ and $CTDI_{vol,0}$ were calculated. Finally, the data were stratified in terms of patient age, sex, and race/ethnicity.

Reporting summary

Further information on research design is available in the Nature Portfolio Reporting Summary linked to this article.

Results
Application to typical scanning and clinical condition

For the case of a typical false positive to true positive ratio of $\beta_0 = 5\%$ and average radiologist interpretative performance of $AUC_0 = 0.75$, the radiation risk among the whole population ranged between 0.0009 and 0.061 deaths per 100 patients (mean: 0.009; median: 0.008); the clinical risk ranged between 0.00007 and 0.094 deaths per 100 patients (mean: 0.045; median: 0.049); and the total risk ranged between 0.002 and 0.146 deaths per 100 patients (mean: 0.053; median: 0.057). Results aggregated by sex and race are reported in Table 2. Figure 1 shows the distribution of radiation, clinical, and total risk for the whole population. The results show that the overall clinical risk exceeds that of radiation risk for the vast majority of cases. This is more evident for Asian patients because they exhibit higher liver cancer related mortality rates according to NCI-SEER program data.

Risk-versus-risk optimization

Concerning the application of the model to estimate the theoretical minimum risk, $R_{t,min}$, Fig. 2 shows two examples of the distributions of radiation, clinical, and total risk with the $CTDI_{vol}$ ranged from 0.1 and 200 mGy with

Table 1 | Number of cases, age, waist diameter, and CTDI_{vol,0} for the simulated population per race and sex

Race	Sex	Number of cases (%)	Age (years) (range); mean; median	Waist diameter (cm) (range); mean; median	CTDI_{vol,0} (mGy) (range); mean; median
Asian	M	26,140 (2.6%)	(0.0, 99.8); 58.8; 60.4	(11, 43.4); 29.6; 29.7	(2.4, 47.3); 13.9; 13.4
	F	31,062 (3.1)	(0.0, 99.9); 60.2; 61.9	(9.5, 43.7); 27.9; 28.1	(2.1, 48.6); 12.1; 11.6
	Total	57,202 (5.7%)	(0.0, 99.9); 59.6; 61.2	(9.2, 43.7); 28.7; 28.9	(2.1, 48.6); 12.9; 12.5
Black	M	49,386 (4.9%)	(0.0, 99.9); 58.1; 60.0	(8.0; 47.7); 32.1; 32.3	(1.8, 50.0); 19.0; 17.1
	F	61,750 (6.2%)	(0.0, 99.9); 60.6; 62.5	(8.0, 50.3); 32.6; 32.8	(1.8, 50.0); 20.3; 17.9
	Total	111,136 (11.1%)	(0.0, 99.9); 59.5; 61.4	(8.0, 50.3); 32.4; 32.6	(1.8, 50.0); 19.7; 17.5
Hispanic	M	58,375 (5.8%)	(0.0, 99.8); 54.9; 55.7	(9.1, 46.8); 32.8; 33.1	(2.0, 50.0); 19.4; 18.4
	F	63,973 (6.4%)	(0.0, 99.9); 57.3; 58.6	(8.4, 46.9); 31.6; 31.9	(1.9, 50.0); 17.7; 16.4
	Total	122,348 (12.2%)	(0.0, 99.9); 56.2; 57.2	(8.4, 46.9); 32.2; 32.5	(1.9, 50.0); 18.5; 17.4
White	M	335,847 (33.6%)	(0.0, 99.9); 63.4; 65.9	(8.1, 48.0); 33.7; 34.0	(1.8, 50.0); 22.1; 19.9
	F	373,467 (37.3)	(0.0, 99.9); 64.9; 67.5	(8.0, 46.3); 31.3; 31.5	(1.8, 50.0); 18.8; 15.8
	Total	709,314 (70.9%)	(0.0, 99.9); 64.2; 66.7	(8.0, 48.0); 32.4; 32.8	(1.8, 50.0); 20.4; 17.9
Total	M	469,748 (47.0%)	(0.0, 99.9); 61.6; 63.8	(8.0, 48.0); 33.2; 33.3	(1.8, 50.0); 21.0; 18.7
	F	530,252 (53.0%)	(0.0, 99.9); 63.2; 65.7	(8.0, 50.3); 31.3; 31.4	(1.8, 50.0); 18.5; 15.7
	Total	1,000,000 (100.0%)	(0.0, 99.9); 62.4; 64.8	(8.0, 50.3); 32.2; 32.4	(1.8, 50.0); 19.7; 17.2

Table 2 | Estimated radiation risk, clinical risk, and total risk per race and sex for the simulated population of 1 million patients, assuming typical false positive to true positive ratio of $\beta_0 = 5\%$ and average radiologist interpretative performance of $AUC_0 = 0.75$. $CTDI_{vol}$ ranged between 1.8 mGy and 50 mGy

| Race	Sex	Radiation risk (mortality per 100 patients) (range); mean; median	Clinical risk (mortality per 100 patients) (range); mean; median	Total risk (mortality per 100 patients) (range); mean; median
Asian	M	(0.002, 0.057); 0.009; 0.008	$(0.004 \times 10^{-1}, 0.076)$; 0.060; 0.067	(0.003, 0.124); 0.069; 0.076
	F	(0.002, 0.051); 0.007; 0.007	$(0.002 \times 10^{-1}, 0.082)$; 0.066; 0.075	(0.002, 0.126); 0.073; 0.084
	Total	(0.002, 0.057); 0.008; 0.007	$(0.009 \times 10^{-1}, 0.082)$; 0.063; 0.071	(0.002, 0.126); 0.071; 0.079
Black	M	(0.001, 0.056); 0.010; 0.009	$(0.007 \times 10^{-2}, 0.080)$; 0.043; 0.044	(0.002, 0.133); 0.053; 0.054
	F	(0.001, 0.052); 0.010; 0.009	$(0.001 \times 10^{-1}, 0.076)$; 0.049; 0.050	(0.003, 0.126); 0.059; 0.060
	Total	(0.001, 0.056); 0.010; 0.009	$(0.007 \times 10^{-2}, 0.080)$; 0.046; 0.045	(0.002, 0.133); 0.056; 0.056
Hispanic	M	(0.002, 0.058); 0.011; 0.011	$(0.002 \times 10^{-1}, 0.094)$; 0.047; 0.045	(0.003, 0.146); 0.058; 0.057
	F	(0.002, 0.052); 0.010; 0.009	$(0.007 \times 10^{-2}, 0.075)$; 0.042; 0.046	(0.002, 0.119); 0.052; 0.056
	Total	(0.002, 0.058); 0.011; 0.010	$(0.007 \times 10^{-2}, 0.094)$; 0.044; 0.045	(0.002, 0.146); 0.055; 0.056
White	M	(0.001, 0.061); 0.010; 0.009	$(0.001 \times 10^{-1}, 0.071)$; 0.043; 0.048	(0.002, 0.128); 0.053; 0.057
	F	$(0.009 \times 10^{-1}, 0.051)$; 0.008; 0.007	$(0.001 \times 10^{-1}, 0.074)$; 0.043; 0.051	(0.002, 0.124); 0.051; 0.058
	Total	$(0.009 \times 10^{-1}, 0.061)$; 0.009; 0.008	$(0.001 \times 10^{-1}, 0.074)$; 0.043; 0.049	(0.002, 0.128); 0.052; 0.057
Total	M	(0.001, 0.061); 0.010; 0.009	$(0.007 \times 10^{-2}, 0.094)$; 0.045; 0.048	(0.002, 0.146); 0.055; 0.057
	F	$(0.009 \times 10^{-1}, 0.052)$; 0.009; 0.007	$(0.007 \times 10^{-2}, 0.082)$; 0.045; 0.051	(0.002, 0.126); 0.053; 0.058
	Total	$(0.009 \times 10^{-1}, 0.061)$; 0.009; 0.008	$(0.007 \times 10^{-2}, 0.094)$; 0.045; 0.049	(0.002, 0.146); 0.054; 0.057
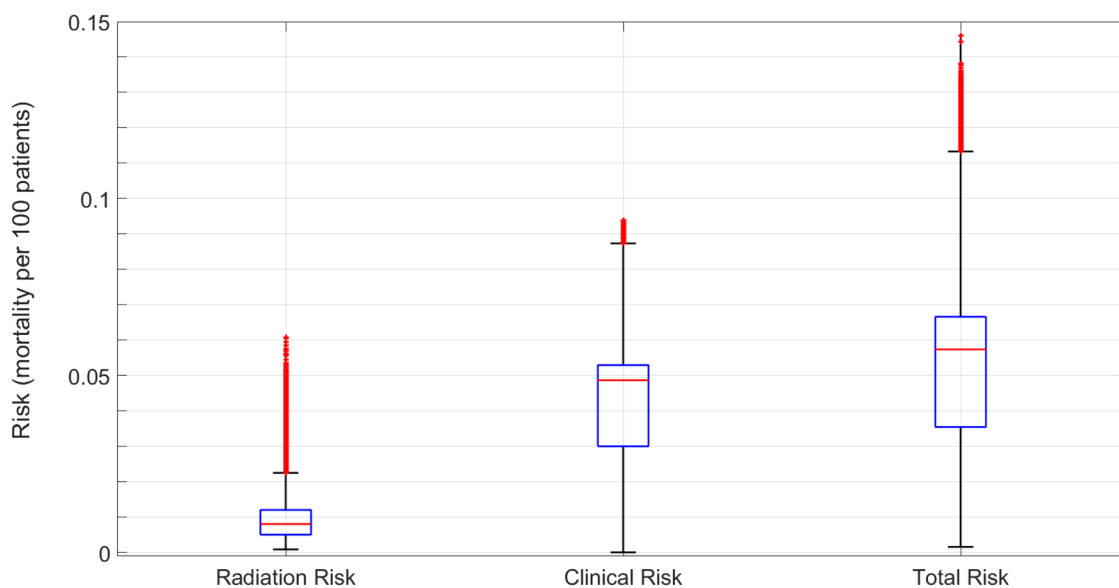
Fig. 1 | Radiation, clinical, and total risks. Distributions of the calculated radiation, clinical, and total risk for the whole population of 1 million patients, assuming typical false positive to true positive ratio of $\beta_0 = 5\%$ and average radiologist interpretative performance of $AUC_0 = 0.75$. $CTDI_{vol}$ ranged between 1.8 mGy and 50 mGy. The red line represents the median and the blue boxes represent the 1st and 3rd quartile. Values that exceed 1.5 times interquartile length (black whiskers) are in red.

0.1 mGy increments and AUC values calculated from Eq. (10). In particular, we show case example of patient n. 561,907 and patient n. 101,174, representing the first and third quartile of theoretical risk reductions (first quartile: 15.9%; third quartile: 2.1%). Moreover, Fig. 3 shows the comparison between the distributions of $CTDI_{vol,0}$ and $CTDI_{vol,min}$, and the related $R_{t,0}$ and theoretical minimum total risk $R_{t,min}$ across the whole population. In this data, $CTDI_{vol,min}$ ranged between 0.1 and 98.2 mGy (mean: 39.8; median: 38.5), and $R_{t,min}$ ranged between 0.0001 and 0.129 deaths per 100 cases (mean: 0.049; median: 0.050). The mean percentage difference between $CTDI_{vol,min}$ and $CTDI_{vol,0}$ was 153.9% (median: 141.8%; min: −99.8%; max: 694.7%) and the average total risk reduction across the whole population was 10.5% (median: 7.4%; min: 0.0%; max: 98.3%). Out of the one million patients, we found 93,242 cases in which the administered $CTDI_{vol,0}$ was higher than the radiation output required to achieve the minimum risk ($CTDI_{vol,min}$)); for 570 cases, the administered $CTDI_{vol,0}$ exactly corresponded to the $CTDI_{vol,min}$; and for the majority of 906,188 cases (90.6%), the administered $CTDI_{vol,0}$ was lower than $CTDI_{vol,min}$.

Figure 4 shows the theoretical minimum total risk for age, sex, and race/ethnicity for the whole population. The jaggedness of the trends is reflective of the expected life-expectancy loss data that are categorized for race/ethnicity, age, and sex[14]. Figure 5 shows the percentage difference between the theoretical minimum total risk $R_{t,min}$ and $R_{t,0}$ versus age for difference sex and race/ethnicity. Figure 6 shows the percentage difference between the administered $CTDI_{vol,0}$ and the radiation output required to achieve the minimum risk ($CTDI_{vol,min}$)) versus age for different sex and race/ethnicity. As reported in Table 3, the Asian female group had the highest total risk reduction potential (−26.6), whereas the Hispanic male group had the lowest (−4.7).
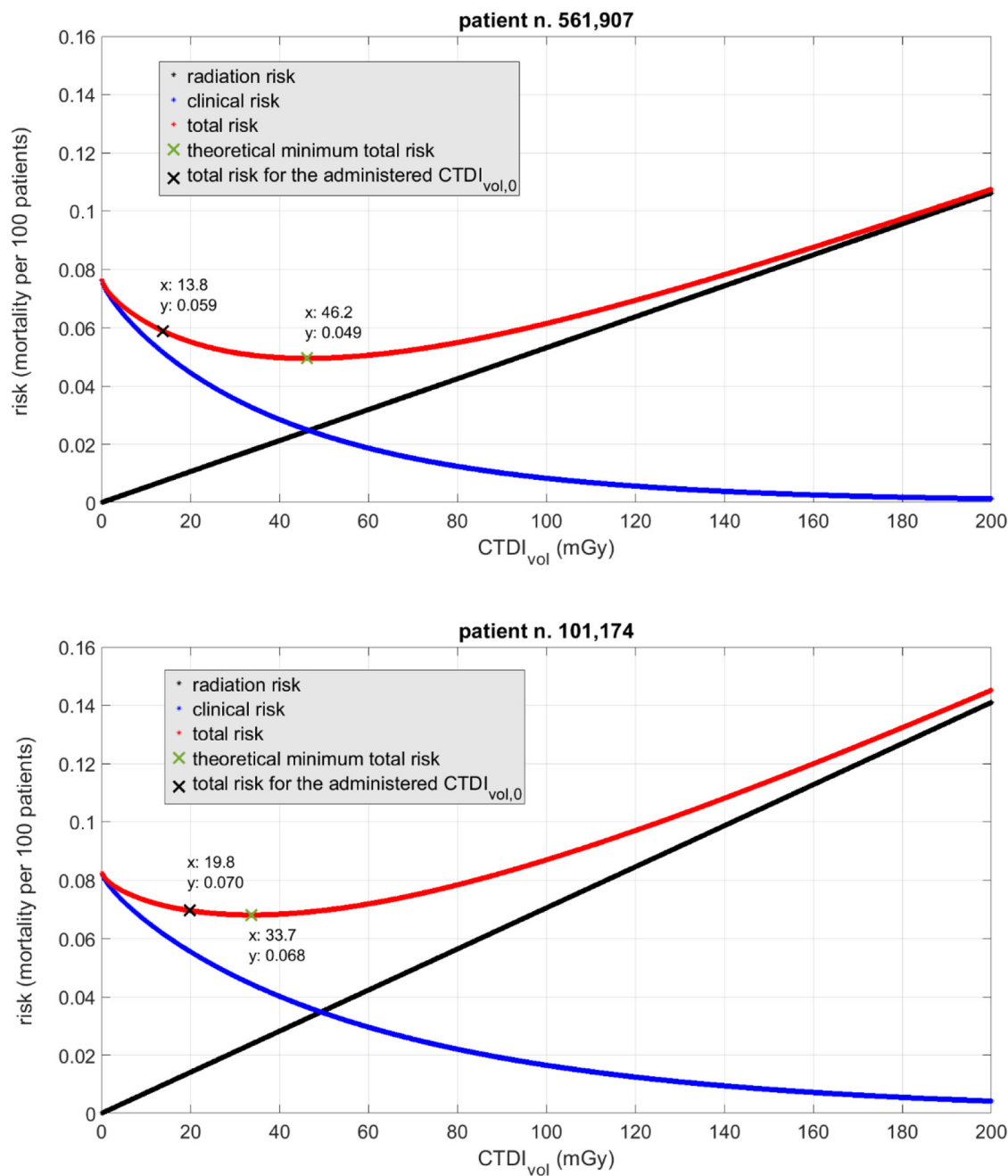
Fig. 2 | Patient examples. Distributions of radiation, clinical, and total risk with the CTDI$_{vol}$ ranged from 0.1 and 200 mGy for patient n. 561,907 and patient n. 101,174, corresponding to the cases for which the first and third quartile theoretical risk reduction was achieved.

Discussion

In this study, we implemented and demonstrated a mathematical model to characterize the interplay between radiation risk and clinical benefit in CT in terms of a risk-versus-risk optimization strategy. Such a framework allows a complete depiction of the total risk associated with an imaging procedure including both the radiation and the clinical risk. To our knowledge, this is the first attempt to define a method that can quantitatively optimize a radiological procedure including its benefit component. We tested the model to a population of one million digital twins simulating a liver cancer scenario. Our estimation in terms of radiation risk are consistent with other studies estimating lifetime attributable cancer mortality risks associated with CT procedures[7,20,21]. In the absence of data describing the clinical risk associated with radiological procedures, our approach provides a theoretical methodology to put the imaging benefit in terms that can be related to radiation risk.

When the model was applied to a scenario reproducing routine scanning condition and typical radiologist interpretative performance (false positive to true positive ratio of $\beta_0 = 5\%$, and $AUC_0 = 0.75$) for a hypothetical liver cancer lesion[17], the results highlighted the dominance of clinical risk. In particular, the clinical risk was found to largely outweigh the radiation risk by a factor of 4 to 5 (Fig. 1, Table 2). This is so in spite of the fact that we used a relatively large radiation dose levels for our modeled imaging scenarios (or CTDI$_{vol}$ of up to 50 mGy), higher than many current low-dose CT practices. This dominance of clinical risk over radiation risk was consistent across population groups, ranging from fourfold in female Hispanic to over ninefold in female Asian patients highlighting the need to incorporate patient demographic in the radiological procedure risk-to-benefit assessment. This is contrary to common assumption about radiation risk that dominates the common understanding of CT safety. Our results in fact emphasize how the over-exaggerated and obsessive understanding of

Fig. 3 | Scanner output and total risk comparisons. Comparison between the distributions of $CTDI_{vol,0}$ and $CTDI_{vol,min}$, and the related $R_{t,0}$ and theoretical minimum total risk $R_{t,min}$ across the whole population. The red line represents the median and the blue boxes represent the 1st and 3rd quartile. Values that exceed 1.5 times interquartile length (black whiskers) are in red.
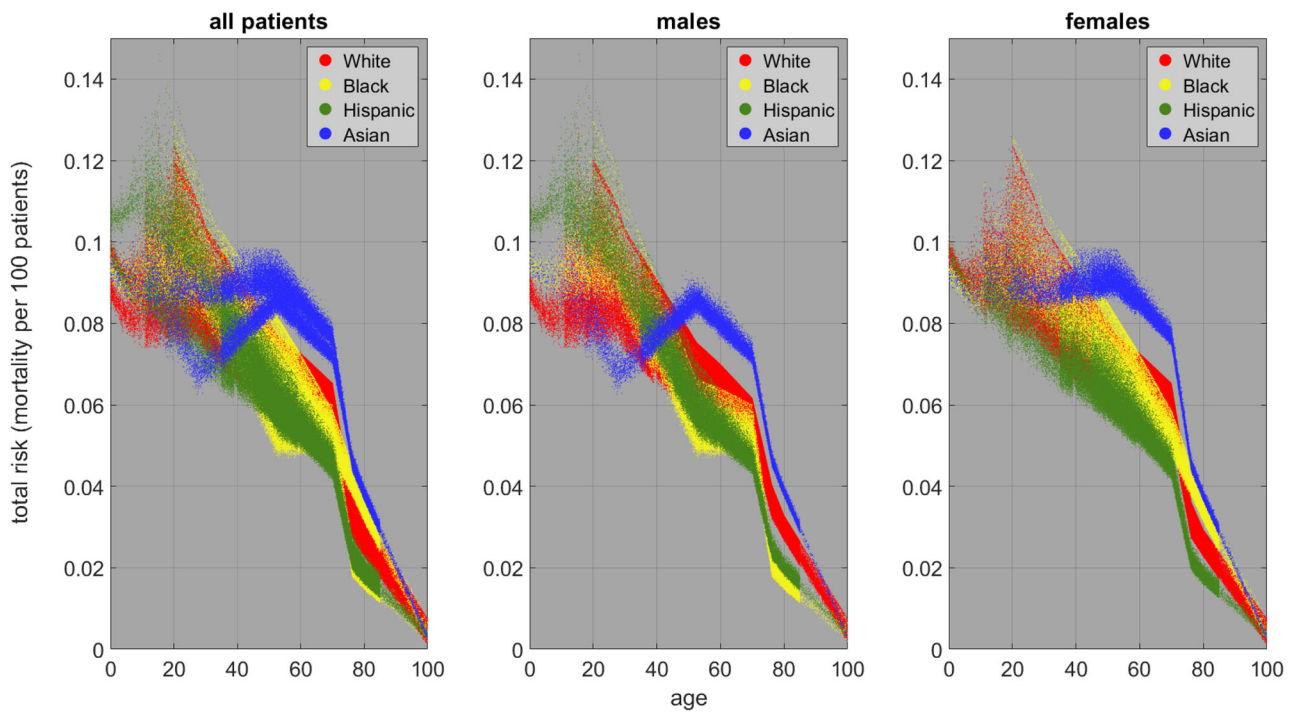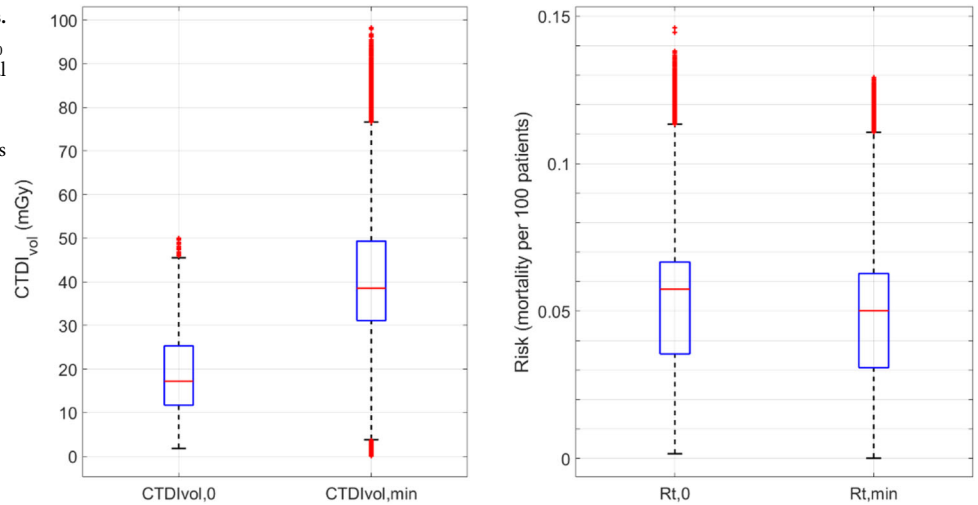

Fig. 4 | Minimum total risk. Theoretical minimum total risk versus age for the whole population (left), male patients (center), and female patients (right). Different colors are different races/ethnicities.

radiation dose, as most recently reflected in the Centers for Medicare and Medicaid Service ruling[22], can impact patient safety negatively.

Assessing the relevance of the mathematical model in the design of optimization strategies, we simulated, 2000 imaging conditions ($CTDI_{vol}$ varying from 0.1 and 200 mGy) per patient, resulting in 2000 different AUC values. Utilizing the distributions of the related radiation, clinical, and total risks, the theoretical minimum total risk $R_{t,min}$ was estimated per patient. The optimum dose level ($CTDI_{vol,min}$) was found be higher than the starting $CTDI_{vol,0}$ in over 90% of the cases implying that, for these procedures, increasing the scanner output could have in fact reduced the overall risk to the patient (Figs. 2, and 3, Table 3). This advantage of increased dose was age-, sex-, and race-dependent, with the highest potential for risk optimization is in the Asian population, with 24% theoretical total risk reduction on average corresponding to a 306% increase in $CTDI_{vol}$; whereas, the Hispanic group showed the lowest average hypothetical total risk reduction of 5% with an 89% scanner output increase.

In the described scenario, it is important to highlight that patient demographic information influence both radiation and clinical risk. In particular, the patient size dictates the scanner X-ray output in exams performed with automated tube current modulation. Moreover, the risk index is calculated by applying age- and sex-specific lifetime attributable risk of cancer incidence coefficients to each organ resulting in a decreasing radiation risk for older patients. Lastly, the clinical risk incorporates the difference between the predicted years of survival for correct and incorrect diagnosis which is also age-, sex-, and race-specific. Such a difference in survival for correct and incorrect diagnosis largely outweighs the stochastic radiation risk resulting in clinical risk dominating the resulting total risk.

Our findings are consistent with what the International Commission of Radiation Protection recommended in publication 135: "Optimization is generally concerned with maintaining the quality of the diagnostic information provided by the examination commensurate with the medical purpose while, at the same time, seeking to reduce patient exposures to
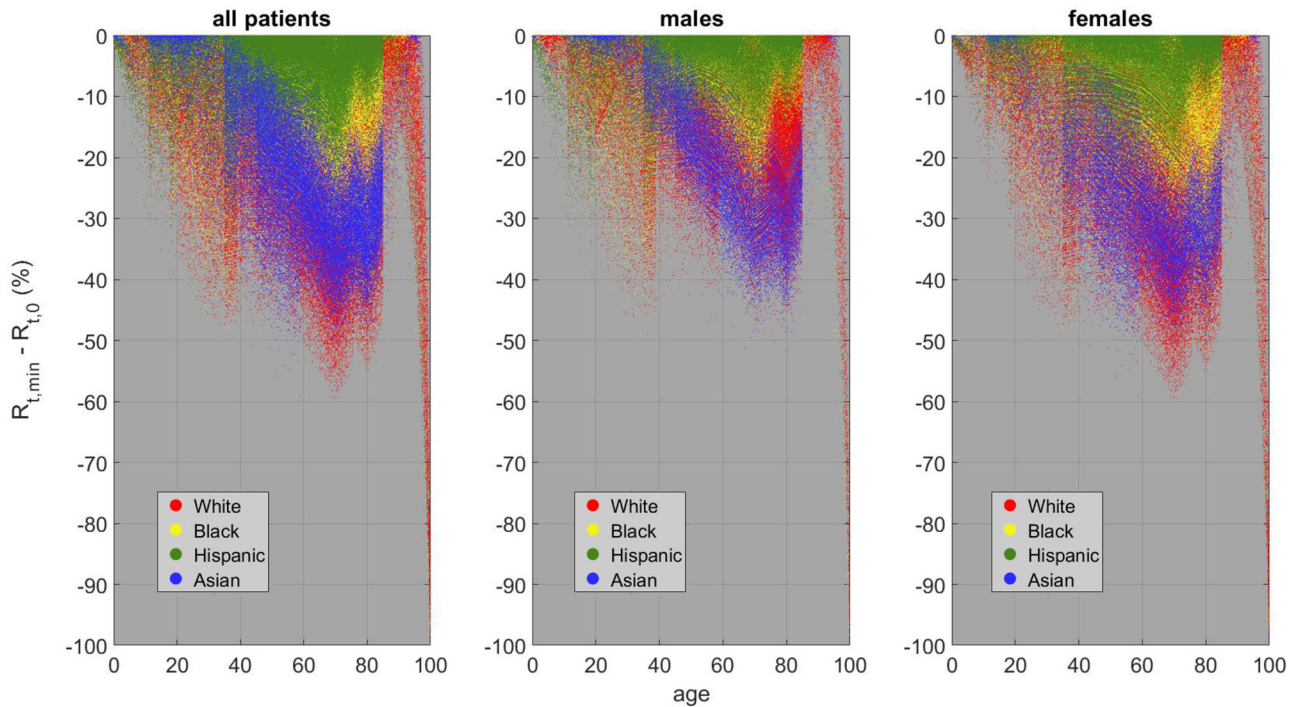
Fig. 5 | Total risk differences. Percentage difference between the theoretical minimum total risk $R_{t,\min}$ and $R_{t,0}$ versus age for the whole population (left), male patients (center), and female patients (right). Different colors are different races/ethnicities.
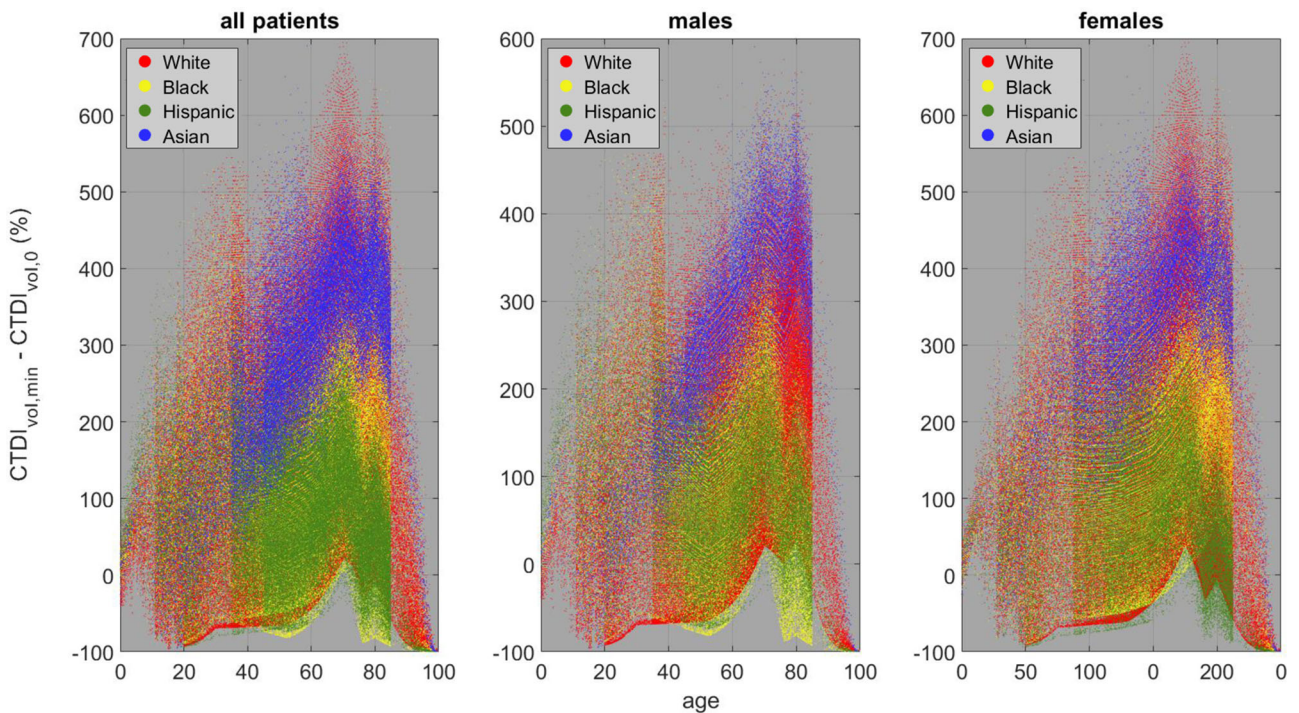

Fig. 6 | Scanner output differences. Percentage difference between the administered $CTDI_{vol,0}$ and the radiation output required to achieve the minimum risk ($CTDI_{vol,\min}$)) versus age for the whole population (left), male patients (center), and female patients (right). Different colors are different races/ethnicities.

radiation to a level as low as reasonably achievable. Image quality or, more generally, the diagnostic information provided by the examination (including the effects of postprocessing) must also be evaluated. […] In some cases, optimization may result in an increase in dose."[23]. This statement represented a paradigm shift in the traditional CT optimization approach that is either based on radiation dose only, or incorporates image quality without quantitatively assessing the resulting clinical outcome[24]. Our

model, instead, proposes a comparison of radiation and clinical risk with comparable units allowing a complete depiction of the total risk associated with a CT procedure and a comprehensive risk-to-benefit assessment.

Our methodology can be considered not only for optimization of imaging procedures but also from the perspective of radiation protection justification. The justification of a medical procedure is meant to be patient-specific, though not always, as in the case of COVID-19 diagnosis or cancer

Table 3 | Percentage differences between $R_{t,min}$ and $R_{t,0}$, and between $CTDI_{vol,min}$ and $CTDI_{vol,0}$ for the simulated population per race and sex

Race	Sex	Difference between $R_{t,min}$ and $R_{t,0}$ (%) (range); mean; median	Difference between $CTDI_{vol,min}$ and $CTDI_{vol,0}$ (%) (range); mean; median
Asian	M	(−83.2, 0.0); −20.6; −21.3	(−99.5, 590.5); 272.7; 289.7
	F	(−92.5, 0.0); −26.6; −27.8	(−99.5, 690.5); 334.6; 348.3
	Total	(−92.5, 0.0); −23.9; −25.0	(−99.5, 690.5); 306.3; 321.9
Black	M	(−98.3, 0.0); −6.2; −3.6	(−99.8, 566.7); 94.3; 94.4
	F	(−96.4, 0.0); −11.2; −9.2	(−99.8, 644.4); 165.9; 163.3
	Total	(−98.3, 0.0); −8.9; −6.1	(−99.8, 644.4); 134.1; 125.7
Hispanic	M	(−95.9, 0.0); −4.7; −3.1	(−99.8, 485.2); 87.9; 83.8
	F	(−97.7, 0.0); −5.3; −3.4	(−99.8, 482.6); 90.3; 87.3
	Total	(−97.7, 0.0); −5.0; −3.3	(−99.8, 485.2); 89.2; 85.6
White	M	(−97.0, 0.0); −8.6; −6.5	(−99.8, 600.0); 134.5; 131.3
	F	(−97.6, 0.0); −12.3; −9.5	(−99.8, 694.7); 175.0; 165.7
	Total	(−97.6, 0.0); −10.6; −7.9	(−99.8, 694.7); 155.8; 147.4
Total	M	(−98.3, 0.0); −8.5; −5.9	(−99.8, 600.0); 132.2; 124.2
	F	(−97.7, 0.0); −12.2; −9.1	(−99.8, 694.7); 173.1; 161.1
	Total	(−98.3, 0.0); −10.5; −7.4	(−99.8, 694.7); 153.9; 141.8

screening where population aggregates have been used[25,26]. The model introduced in this study can help to better inform the justification of an exam both for the single individual and for a population (e.g., an exam might be justified for an ethnic group and sex, but not for another).

This study had a few limitations. First, while we equated radiation and clinical risks through identical units, they are associated with different timeframes: the risk related to radiation exposures is associated with the adverse effects in years and decades, whereas the clinical risk is associated with the specific pathology progression that tends to have shorter timespans. The proposed model should be extended to include differing time horizons. Second, our study focused on only one clinical task associated with liver cancer. The framework can be extended to other diagnostic tasks. To do so, one can designate a "most difficult task" as the limiting task of a protocol, thus ordain the optimization process for imaging of that body part. Third, the described method does not include many potential additional or ancillary clinical variables that are patient specific and may weigh in when deciding the appropriateness of an imaging procedure. Fourth, this study did not associate any uncertainties to the calculated quantities. Currently, only models describing radiation risk uncertainties are available, and it has been reported that the averaged relative error for risk index in abdomino-pelvic examinations is 0.2[7]. Future studies can aim to assess the overall total risk uncertainties. Lastly, the false positive to true positive ratio of $\beta_0 = 5\%$, and $AUC_0 = 0.75$ were chosen to describe typical radiologist interpretative performance on a typical, relevant cancer detection task. Although these are reasonable assumptions[17], different practices can be represented by different β_0 and AUC_0 values, thus leading to different results. Nevertheless, the validity of the proposed model is not impacted by the specific interpretative performance and can be applied to any set of targeted false positive to true positive ratio and area under the ROC curve.

Conclusion

A mathematical framework to describe total risk in CT was implemented and robustly tested in a simulated dataset of 1,000,000 CT studies reproducing a clinical liver cancer detection scenario. Framing risk-to-benefit assessment as a risk-versus-risk question, calculating both clinical and radiation risk using comparable units, allows a quantitative depiction of total risks in CT. Yielding differing results across patient age and race stratifications, the results highlighted the dominance of clinical risk at typical CT

examination dose levels and that, in the current practice, there is room for increase in radiation dose to the benefit of the patient. Further, exaggerated dose reductions beyond current levels can even harm patients. Care should be exercised that any dose reduction should not be done at the expense of quality patient care, and the mathematical model demonstrated in this study can aid in quantitative individualized justification and optimization of imaging exams.

Data availability

All data generated and analyzed in the study (source data) are publicly available via the CERN's Zenodo repository (https://doi.org/10.5281/zenodo.13715861)[27]. Particularly, the dataset includes the data summarized in all the tables and the figures reported in this manuscript. Any publication of results obtained with this dataset should reference this paper. Moreover, the demographic and anatomical information taken from the 2019 Census Population Estimates[15] and from the Center for Disease Control and Prevention Anthropometric Reference Data for Children and Adults: United States 2015–2018[16], are publicly available. Any further information about data calculation and analysis is available from the corresponding author on reasonable request.

References

1. Basic Safety Standards. *GSR part 3*. International Atomic Energy Agency, Vienna **3**, 471 (2014).
2. Icrp. The 2007 Recommendations of the International Commission on Radiological Protection. ICRP Publication 103. Annals of the ICRP **37**, 9–34. (2007).
3. Samei, E. et al. Medical imaging dose optimisation from ground up: expert opinion of an international summit. *J. Radiol. Prot.* **38**, 967–989 (2018).
4. NCRP. NCRP. *National Council on Radiation Protection and Measurements. Medical Radiation Exposure of Patients in the United Stated (2019)*, (2019). NCRP Report no. 184. 2019. Report No.: ISBN: 9781944888169.
5. McCollough C., et al. *AAPM report n.96. The Measurement, Reporting, and Management of Radiation Dose in CT, The Report of AAPM Task Group 23*. College Park, MD; 2008.
6. Valentin, J. Managing patient dose in multi-detector computed tomography(MDCT). ICRP Publication 102. *Ann. ICRP* **37**, 1–79 (2007).
7. Ria, F. et al. Comparison of 12 surrogates to characterize CT radiation risk across a clinical population. *Eur. Radiol.* **31**, 7022–7030 (2021).
8. Cheng, Y. et al. Validation of algorithmic CT image quality metrics with preferences of radiologists. *Med. Phys.* **46**, 4837–4846 (2019).
9. Cheng, Y., Smith, T. B., Jensen, C. T., Liu, X. & Samei, E. Correlation of algorithmic and visual assessment of lesion detection in clinical images. *Acad. Radiol.* **27**, 847–855 (2020).
10. Smith, T. B., Solomon, J. & Samei, E. Estimating detectability index in vivo: development and validation of an automated methodology. *J. Med. Imaging* **5**, 1–9 (2017).
11. Icrp. Radiation protection in medicine. ICRP Publication 105. *Ann. ICRP*. 2007.
12. Li, X. et al. Patient-specific radiation dose and cancer risk estimation in CT: part II. Application to patients. *Med. Phys.* **38**, 408–419 (2011).
13. *Health Risks from Exposure to Low Levels of Ionizing Radiation: BEIR VII Phase 2*. (Washington, D.C.: National Academies Press, 2006).
14. National Cancer Institute Surveillance E, and End Results Program. SEER*Explorer: An interactive website for SEER cancer statistics. Surveillance Research Program, National Cancer Institute; 2023 Apr 19. 2023 https://seer.cancer.gov/statistics-network/explorer/.
15. Census.gov. 2019 Population Estimates by Age, Sex, Race and Hispanic Origin: Census.gov; 2020 https://www.census.gov/newsroom/press-kits/2020/population-estimates-detailed.html.

16. Fryar CDC, M.D.; Gu, Q.; Afful, J.; Ogden, C.L. Anthropometric reference data for children and adults: United States, 2015–2018. Washington, DC: National Center for Health Statistics; 2021.

17. Mileto, A. et al. CT detectability of small low-contrast hypoattenuating focal lesions: iterative reconstructions versus filtered back projection. *Radiology* **289**, 443–54 (2018).

18. Rolland, J. P. & Barrett, H. H. Effect of random background inhomogeneity on observer detection performance. *J. Opt. Soc. Am. A.* **9**, 649–58 (1992).

19. Barrett, H. H., Myers, K. J., Hoeschen, C., Kupinski, M. A. & Little, M. P. Task-based measures of image quality and their relation to radiation dose and patient risk. *Phys. Med. Biol.* **60**, R1 (2015).

20. Zewde, N., Ria, F. & Rehani, M. M. Organ doses and cancer risk assessment in patients exposed to high doses from recurrent CT exams. *Eur. J. Radiol.* **149**, 110224 (2022). (February).

21. Bosch de Basea Gomez, M. et al. Risk of hematological malignancies from CT radiation exposure in children, adolescents and young adults. *Nat. Med.* **29**, 3111–9 (2023).

22. Excessive radiation dose or inadequate image quality for diagnostic computed tomography (CT) in adults (Facility IQR), CMS1074v1 (2023).

23. Vañó, E. et al. ICRP Publication 135: diagnostic reference levels in medical imaging. *Ann. ICRP* **46**, 1–144 (2017).

24. McCollough, C. H. & Leng, S. Use of artificial intelligence in computed tomography dose optimisation. *Ann. ICRP* **49**, 113–25 (2020).

25. Ria F. et al. A comparison of COVID-19 and imaging radiation risk in clinical patient populations. *J. Radiol Prot.* 40, 1336–1345 (2020).

26. Rubin, G. D. et al. The role of chest imaging in patient management during the COVID-19 pandemic: a multinational consensus statement from the Fleischner Society. *Radiology* **296**, 172–80 (2020).

27. Ria F. Optimization of abdominal CT based on a model of total risk minimization by putting radiation risk in perspective with imaging benefit. Zenodo. https://doi.org/10.5281/zenodo.13715861 (2024).

Acknowledgements

Author contributions
F.R.: Conceptualization, Data curation, Formal analysis, Investigation, Methodology, Project administration, Visualization, Writing – original draft, Writing – review & editing. A.R.Z.: Conceptualization, Data curation, Formal analysis, Methodology, Writing – review & editing. R.L.: Conceptualization, Data curation, Formal analysis, Methodology, Writing – review & editing. A.E.: Data curation, Formal analysis, Methodology, Writing – review & editing. E.A.: Methodology, Formal analysis, Writing – review & editing. E.S.: Conceptualization, Supervision, Investigation, Methodology, Visualization, Writing – review & editing.

Competing interests
The authors declare no competing interests.

Additional information